Supporting Information

for

Integrated dual-confinement effects of quantum dots and spatial CO_2 activation for enhanced photoreduction performance

Jia Zheng, [a] Xiaoxue Zhao, [b] Yang Li, [c] Zhengguo Song, [c] and Zhi Liu*[c]

[a] *College of Chemistry, Changchun Normal University, Changchun 130032, P.R. China*

[b] *College of Chemical Engineering, Hebei Normal University of Science & Technology, Qinhuangdao 066004, P.R. China*

[c] *Faculty of Chemistry and Chemical Engineering, Shantou University, Shantou 515063, P.R. China*

*Corresponding authors: Tel.: +86 754 86503791; fax: +86 754 82902767.

E-mail address: zhiliu@stu.edu.cn

1. Materials and reagents

Chemical agents were purchased from Sinopharm Chemical Reagent Co., Ltd., and all of them were used without any further purification. These agents include $C_4H_6CoO_4 \cdot 4H_2O$, $Na_2S \cdot 9H_2O$, $Ni(NO_3)_3 \cdot 6H_2O$, $Al(NO_3)_3 \cdot 9H_2O$, urea, and NH_4F. Deionized water was used to prepare different solutions and rinse samples.

2. Preparation of samples

2.1 Preparation of NiAl-LDH

A total of 0.3753 g of $Al(NO_3)_3 \cdot 9H_2O$ and 0.8724 g of $Ni(NO_3)_2 \cdot 6H_2O$ were dissolved in 60 mL of deionized water under stirring. Subsequently, 0.296 g of urea and 1.2012 g of NH_4F were added to the solution and stirred for an additional 30 min. The obtained homogeneous solution was then transferred into a 100 mL Teflon-lined stainless-steel autoclave and subjected to hydrothermal treatment at 120 °C for 24 h. After cooling to room temperature, the resulting precipitate was collected by centrifugation, washed several times with deionized water and ethanol, and dried in an oven at 80 °C for 24 h to obtain NiAl-LDH.

2.2 Preparation of Co_3S_4 QDs

A total of 0.249 g of $C_4H_6CoO_4 \cdot 4H_2O$ was dissolved in 60 mL of deionized water under stirring. Subsequently, 1.2 g of Na_2S was added to the solution, followed by vigorous stirring to ensure thorough mixing. The resulting mixture was then transferred into an 80 mL Teflon-lined stainless-steel autoclave and subjected to hydrothermal treatment at 120 °C for 20 h. After naturally cooling to room temperature, the obtained black precipitate was collected by centrifugation, washed

several times with deionized water and ethanol, and dried at 60 °C for 2 h to yield Co_3S_4 quantum dots, denoted as Co_3S_4 QDs

2.3 Preparation of CSL photocatalysts

A total of 0.06 g of the as-prepared Co_3S_4 QDs and 1.00 g of NiAl-LDH were dispersed in 60 mL of ethanol, followed by vigorous stirring in a water bath at 70 °C until the ethanol was completely evaporated. The obtained composite powder was denoted as CSL-6. Similarly, by adjusting the amount of Co_3S_4 QDs to 0.02 g, 0.04 g, 0.08 g, and 0.10 g while keeping other conditions unchanged, four additional samples were synthesized using the same procedure and denoted as CSL-2, CSL-4, CSL-8, and CSL-10, respectively.

3. Characterizations

The crystal structure of the samples was performed on SHIMADZU XRD-6100X-ray powder diffraction (XRD) with Cu Kα radiation (λ = 0.154598 nm) at 40 kV voltage, 40 mA current, 10° min^{-1} scan rate and 2θ range of 10°-80°. Raman spectra were performed on a laser Raman spectrometer (Invia Reflex) with an excitation wavelength of 633 nm. JEM2100F Higher-Resolution Transmission Electron Microscopy (HRTEM**)**, while recorded the mapping and the energy dispersive spectrometer **(**EDS**)** by HR-TEM. X-ray photoelectron spectroscopy **(**XPS**)** analysis was assessed through a PHI Quantum 2000 XPS system with C 1s (284.8 eV) as calibration. Ultraviolet-visible diffuse reflectance spectra (UV-vis DRS) of samples were investigated by Agilent Cary 500 UV-vis spectrophotometer using $BaSO_4$ as reference. An electrochemical workstation (CHI 660D, Shanghai Chen Hua

Instrument Co, Ltd, China) with a standard three-electrode system contained 0.5 M Na_2SO_4 electrolyte was used to carry out the Mott-Schottky spots (at frequency of 1500 Hz, 2000 Hz, 2500 Hz), photocurrent (was executed from frequency of 10^6 to 10^1 Hz with applying 0 biases under visible light irradiation at open-circuit potential) and EIS spectra, and the samples coated on ITO glass (2 × 2 cm^2) served as working electrodes. Photoluminescence (PL) spectra and the time-resolved photoluminescence (TRPL) decay spectra were performed on a QuantaMasterTM 40 spectrofluorometer.

4. CO_2 photoreduction measurements

CO_2 photoreduction performance of the as-prepared photocatalysts was evaluated in a lab-built two-neck quartz photoreactor. Typically, 10 mg of photocatalyst was loaded into the reactor. After removing residual air by continuously introducing high-purity CO_2 (99.999%) and water vapor for 20 min, the reactor was irradiated with a 300 W Xe lamp equipped with an AM 1.5G filter (100 mW·cm^{-2}) for 4 h at 25 °C. The main gas phase products were analyzed by a gas chromatography (GC-7920), which is outfitted with a flame ionization detector with N_2 as the carrying gas. The apparent quantum efficiency (AQE) is calculated using the following formula:

$$AQE(\%) = \frac{2N(CO)}{N_{photon}}$$

$$N_{photon} = \frac{light\ intensity\left(\frac{\mu W}{cm^2}\right) \times illumination\ area\ (cm^2) \times illumina}{N_A(6.02 \times 10^{23}) \times \frac{h(J \cdot s) \times c(m/s)}{\lambda(m)}}$$

where N(CO) represent the yield amount of CO; N_A is Avogadro's constant; h is the

Planck constant; c is the speed of light, and λ is the wavelength.

5. In-situ DRIFTS measurements

In-situ DRIFTS spectra were detected by using a Thermo Scientific Nicolet iS50, equipped with an MCT detector cooled by liquid nitrogen and a commercial reaction chamber from Harrick Scientific. Before measurement, the sample was treated at 80 ^{o}C under vacuum to remove the adsorbed contaminants. The DRIFTS spectrum in the dark was first collected as the background prior to any gas introduction. Next, CO_2 adsorption on the sample was performed in the dark after continuous flow of a mixture of CO_2 and H_2O vapor for 30 min. Then, the reactor was illuminated with a LED-lamp for 40 min to obtain consecutive spectrum data.

6. Density functional theory (DFT) calculations method

The electron exchange and correlation were described with GGA-RPBE functional.[S1, S2] The localized double-numerical quality basis set with a polarization d-function (DNP-4.4 file) was chosen to expand the wave functions.[S3, S4] The core electrons of the metal atoms were treated using the effective core potentials (ECP), and the orbital cutoff was 3.5 Å for all atoms. For the geometry optimization, the convergences of the energy, maximum force, and maximum displacement were set as 2×10^{-5} Ha, 4×10^{-3} Ha/Å, and 5×10^{-3} Å, and the SCF convergence for each electronic energy was set as 1.0×10^{-5} Ha. The K-points was set 7×6×1 in all the geometrical calculation for ensuring accuracy, calculating the density of state (DOS), including PDOS, the K-point also were set the value. The vibrational frequency analysis was performed to gain the thermodynamic results. According to the vibrational analysis,

the correlation of thermodynamic parameters (with the zero-point energy included) of the free energy (ΔGcorr) was taken into consideration in the study of the reaction mechanism.[S5] The free energy at specific temperature were calculated by the formula G = Etotal + Gcorr, where Etotal is the total energy of the specific molecular and Gcorr is the free energy correlation with the zero-point energy included at the specific temperature. So, the related free energy change at 298.15 K in each step is obtained by using the equation ΔG = ΔEtotal + ΔGcorr, where ΔEtotal is the energy difference of the total energy between each species, and ΔGcorr is the energy difference of the free energy correlations at 298.15 K. Representative slab/interface models of NiAl-LDH, Co_3S_4 and Co_3S_4/NiAl-LDH were constructed for comparative calculations. The exposed surfaces were selected based on experimentally observed lattice fringes and representative low-index configurations. A vacuum layer perpendicular to the slab was used to avoid interactions between periodic images. For CO_2 and key intermediates, several possible adsorption configurations at Co/S sites, hydroxyl-rich LDH sites and interfacial sites were optimized, and the most stable configurations were selected for charge-density-difference and free-energy analyses.

Figures:

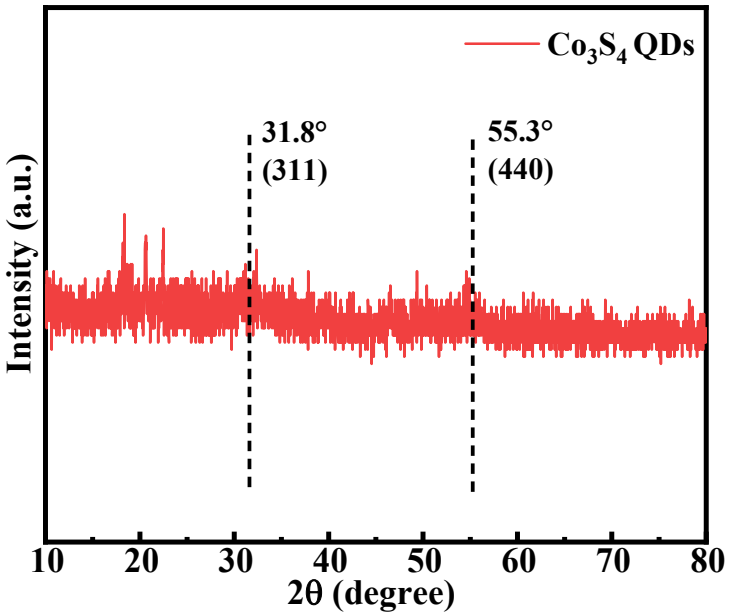

Fig. S1 XRD pattern of Co_3S_4 QDs

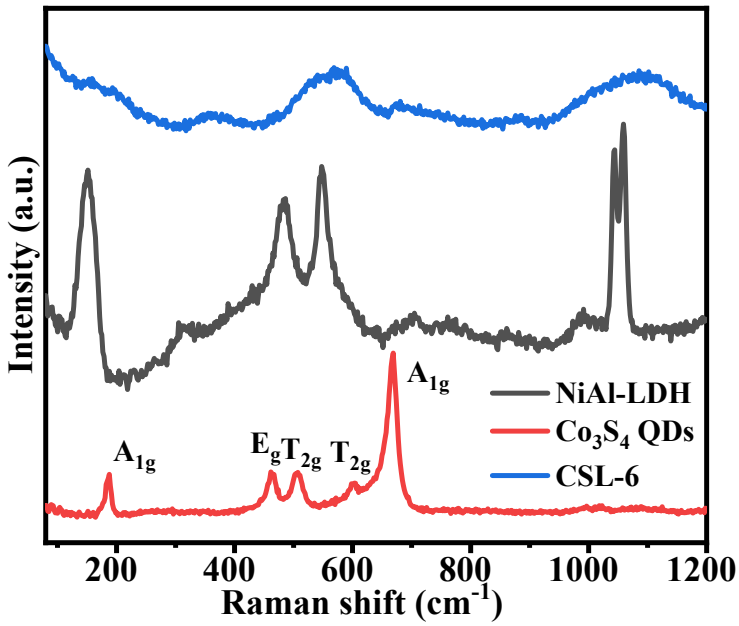

Fig. S2 Raman spectra of pristine NiAl-LDH, Co_3S_4 QDs, and CSL-6

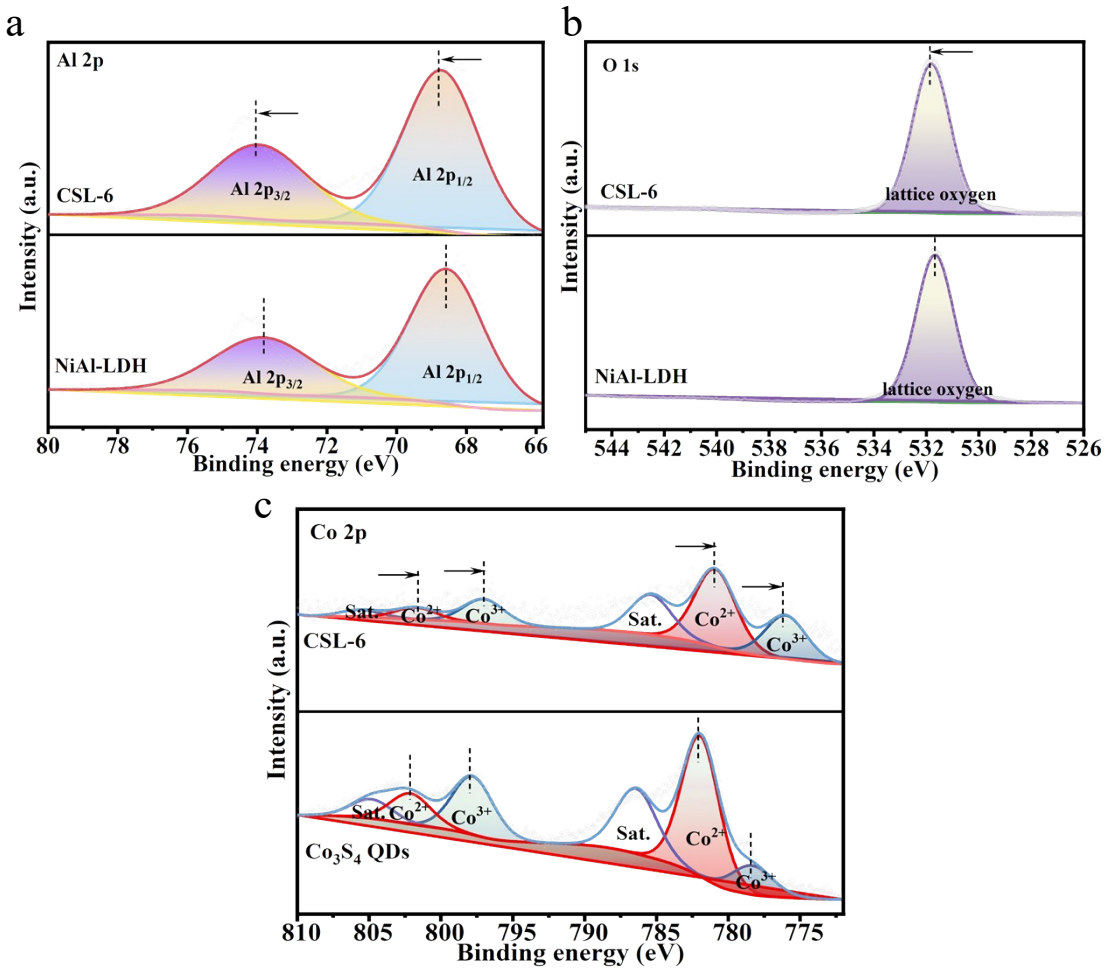

Fig. S3 High-resolution XPS spectra of Al (a), O (b), and Co (c)

in pristine NiAl-LDH and CSL-6

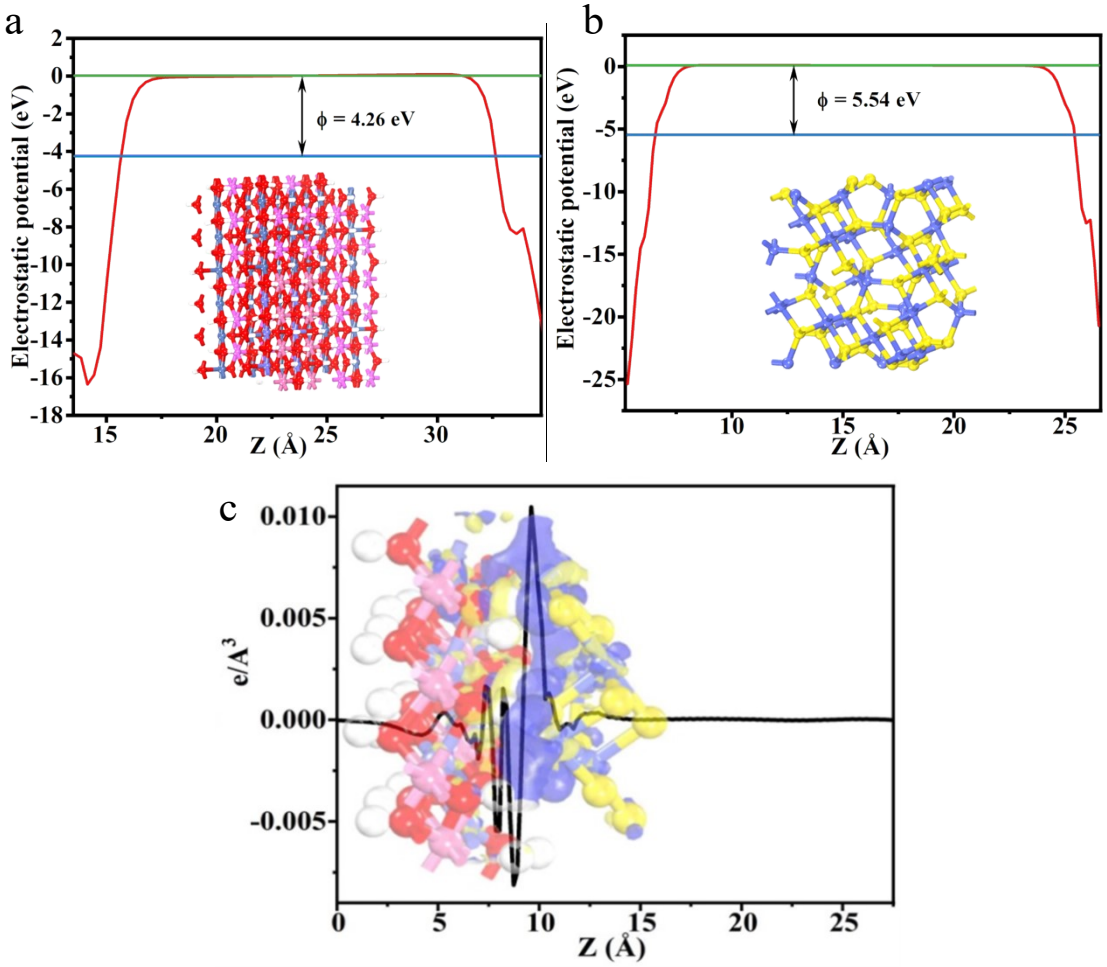

Fig. S4 Calculated work functions of (a) pristine NiAl-LDH and (b) Co_3S_4 QDs, (c) charge integration of $\Delta\rho$ for CSL-6

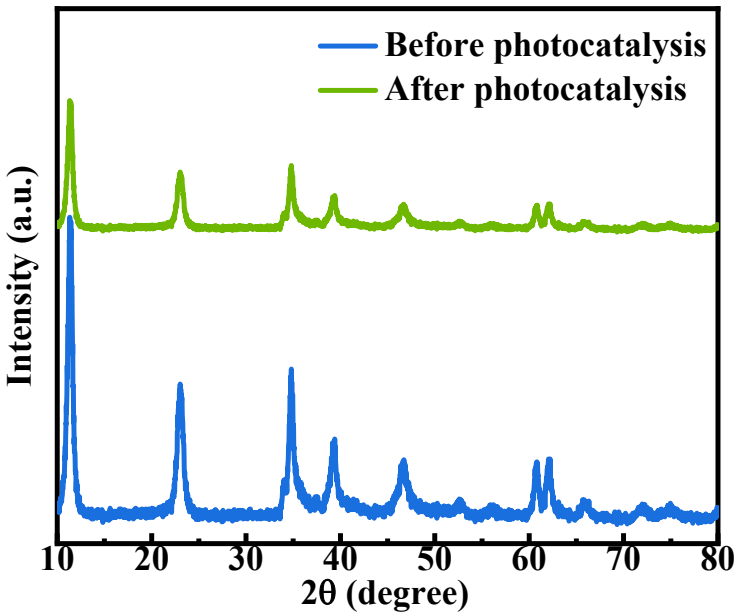

Fig. S5 XRD patterns of CLS-6 before and after photocatalysis

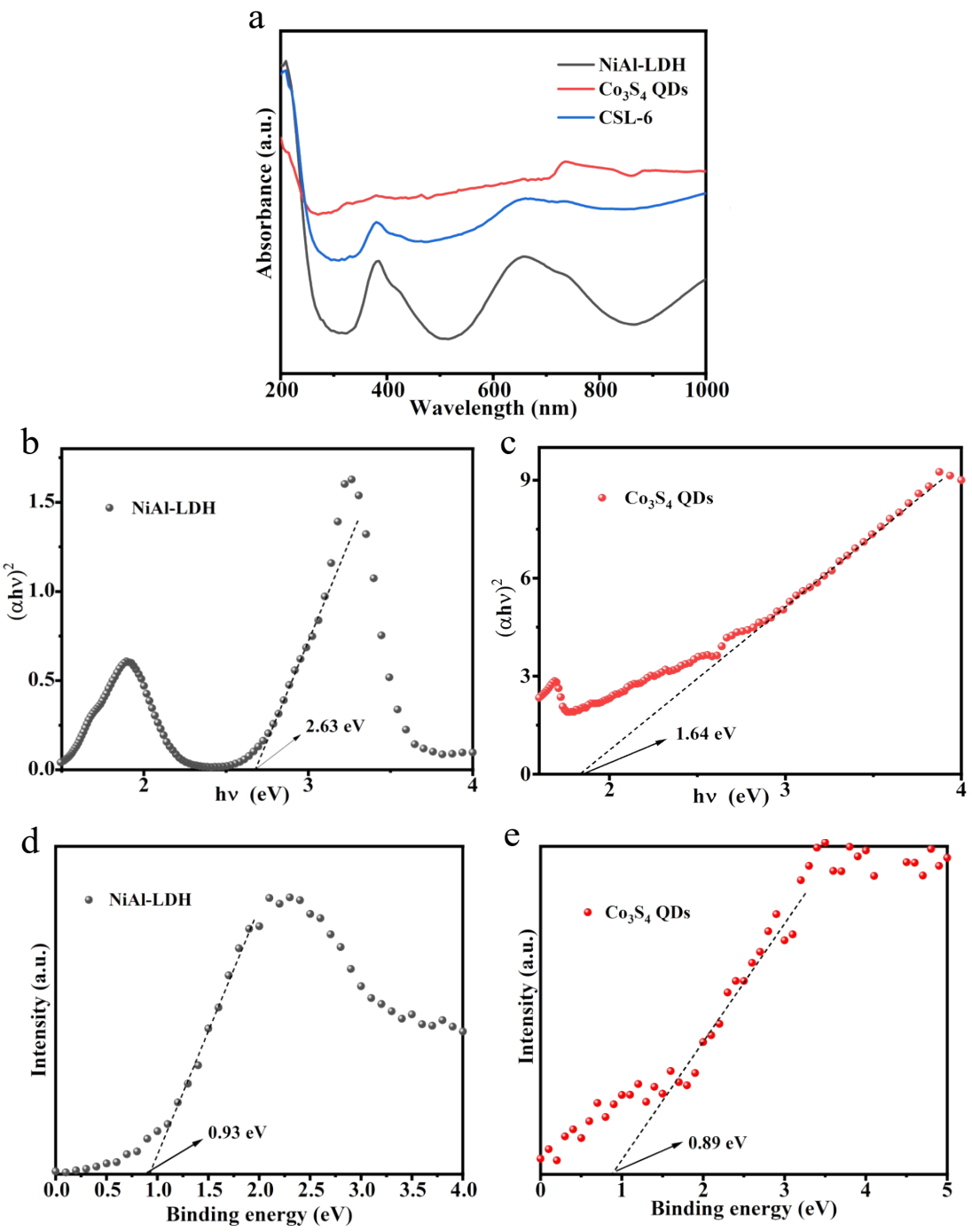

Fig. S6 (a) UV-vis spectrum of pristine NiAl-LDH, Co_3S_4 QDs, and CSL-6, corresponding Tauc plots of $(ahυ)^2$ *vs.* (hυ) of (b) pristine NiAl-LDH and (c) Co_3S_4 QDs, and XPS VB spectra of (d) pristine NiAl-LDH and (e) Co_3S_4 QDs

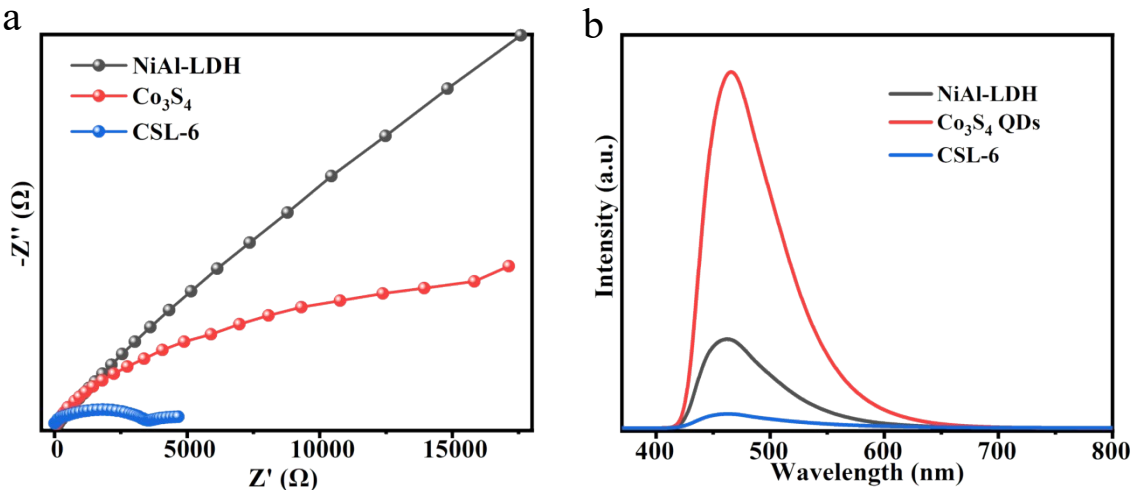

Fig. S7 (a) (c) EIS plots and (b) PL spectra of pristine NiAl-LDH, Co_3S_4 QDs, and CSL-6

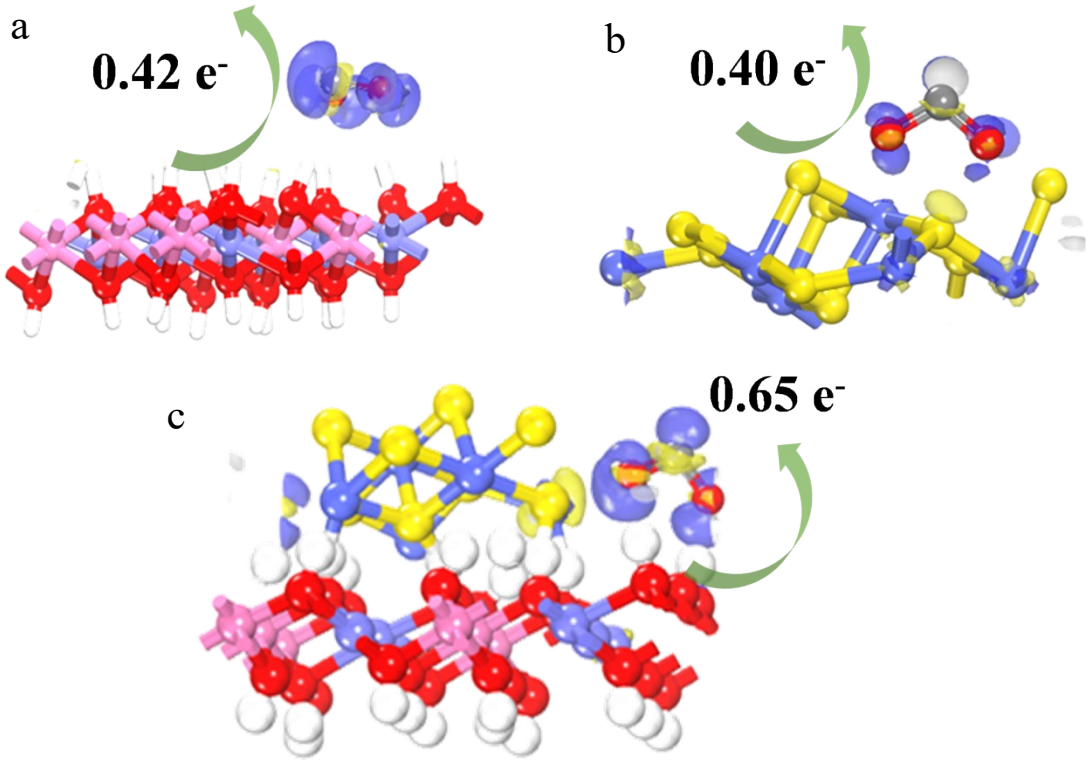

Fig. S8 (a) Pristine NiAl-LDH, (b) Co_3S_4 QDs, and (c) CSL-6 with adsorbed CO_2 structure model

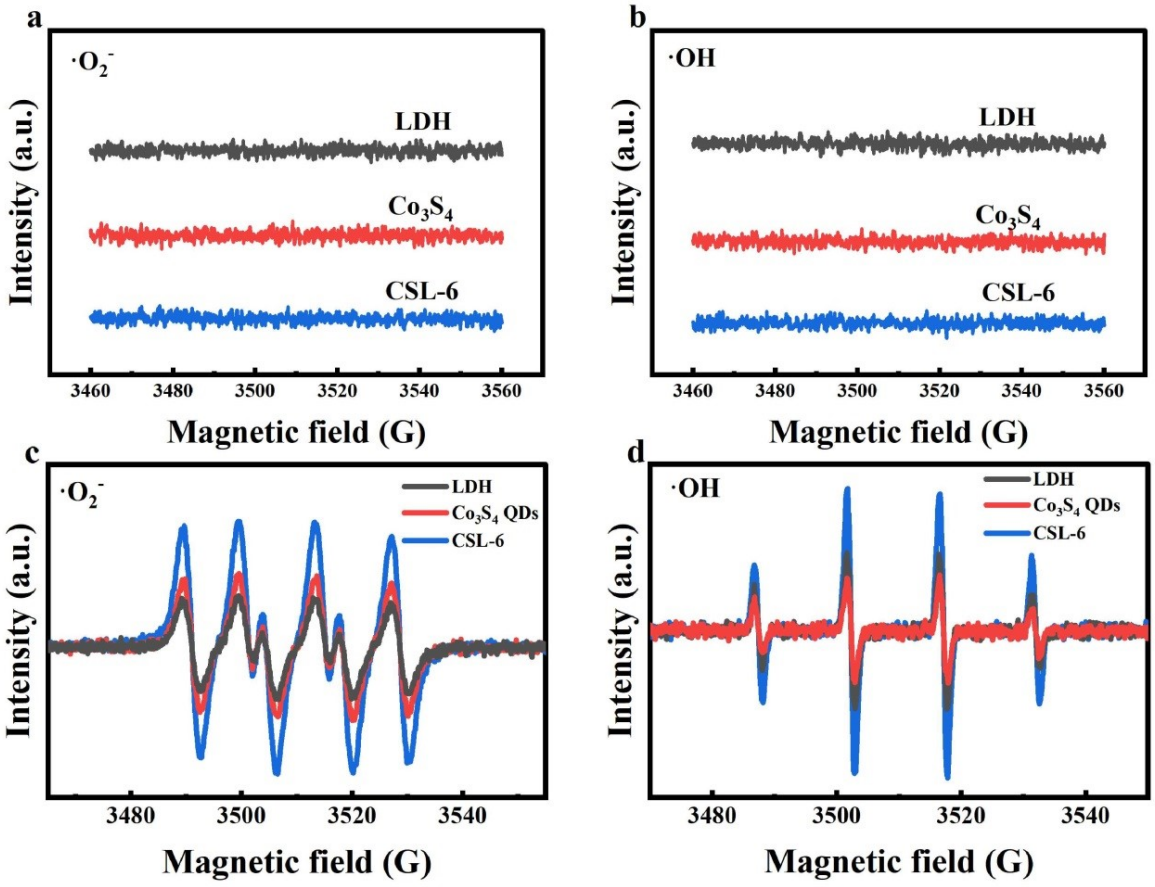

Fig. S9 EPR spectra for DMPO-•O_2-in dark (a) and light (c), DMPO-•OH in dark (b) and light (d)

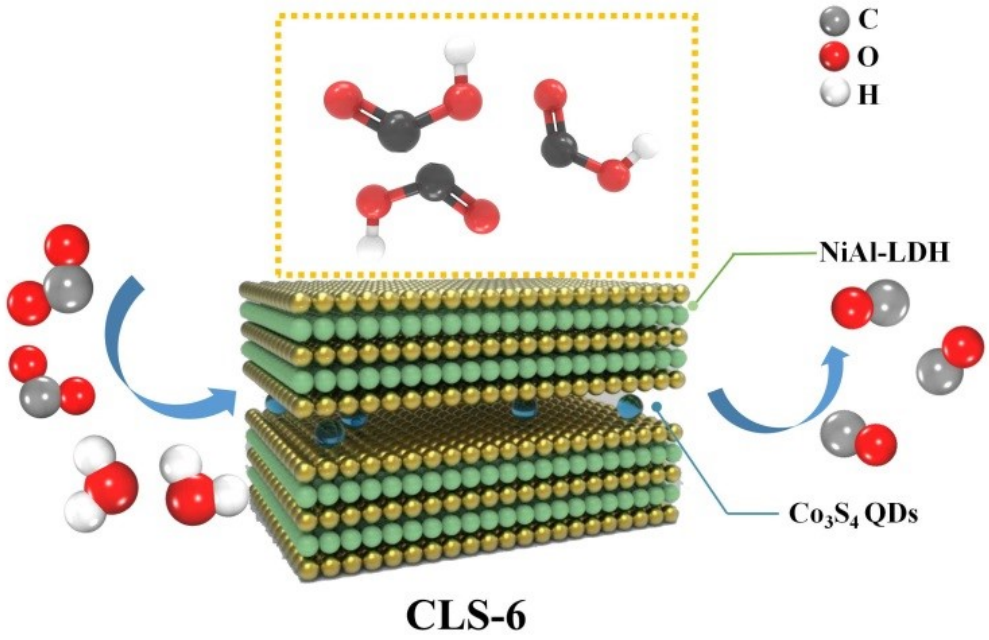

Fig. S10 Schematic mechanism illustration of CO_2 photoreduction to CO over CSL-6

Table S1 Comparison of photocatalytic CO_2 reduction performance over representative NiAl-LDH-based and CoS*x*-based photocatalysts

Catalyst	Light source	Main product	yield rate (umol $h^{-1} \cdot g^{-1}$)	Ref.
CLS-6	**AM 1.5G**	**CO**	**31.2**	**This work**
g-C_3N_4/NiAl-LDH	$\lambda \geqslant 420$ nm	CO	8.2	S6
Urchin-like g-C_3N_4/NiAl-LDH	Xe lamp (300 W)	CO	27.02	S7
NiAl-LDH/g-C_3N_4/CQDs	Xe lamp (300 W)	CO	5.2	S8
NALDH/CN/GA-20	Xe lamp (300 W)	CO	28.83	S9
CQDs/$Bi_{12}O_{17}Cl_2$/NiAl-LDH	Xe lamp (300 W)	CO	16.4	S10
Co_3S_4/NC@ZnS/NC	Xe lamp (300 W)	CO	28.44	S11
Co-Co_3S_4@NC	Xe lamp (300 W)	CO	23.14	S12

S1 J. Kim, T. Lee, H. D. Jung, M. Kim, J. Eo, B. Kang, H. Jung, J. Park, D. Bae, Y. Lee, S. Park, W. Kim, S. Back, Y. Lee and D. H. Nam, *Nat. Commun.*, 2024, **15**, 192.

S2 B. H. Deng, Z. L. Chen, L. X. Yang, J. W. Guo, C. Cheng, X. F. Li, S. Q. Zhang and S. L. Luo, *J. Hazard. Mater.*, 2024, **466**, 133606.

S3 F. Fan, Z. P. Chen, A. N. Zhou, Z. Y. Yang, Y. T. Zhang, X. X. He, J. Kang and W. W. Zhou, *Fuel*, 2023, **333**, 126351.

S4 C. Liao, J. M. Kasper, A. J. Jenkins, P. Yang, E. R. Batista, M. J. Frisch and X. S. Li, *JACS Au*, 2023, **3**, 358-367.

S5 Y. Pan, Y. J. Chen, K. L. Wu, Z. Chen, S. J. Liu, X. Cao, W. C. Cheong, T. Meng, J. Luo, L. R. Zheng, C. G. Liu, D. S. Wang, Q. Peng, J. Li and C. Chen, *Nat. Commun.*, 2019, **10**, 4290.

S6 S. Tonda, S. Kumar, M. Bhardwaj, P. Yadav and S. Ogale, *ACS Appl. Mater. Interf.,* 2018, **10**, 2667-2678.

S7 Q. R. Shi, J. J. Huang, Y. Yang, J. J. Wu, J. Y. Shen, X. D. Liu, A. W. Sun and Z. L. Liu, *Mater. Lett*., 2020, **268**, 127560.

S8 W. T Liu, Q. Wang, Z. Liu, G. X. Ding, *J. Colloid Interf. Sci.* 2022, **622**, 21-30.

S9 M. Yang, P. Wang, Y. J. Li, S. P. Tang, X. Lin, H. Y. Zhang, Z. Zhu, F. T. Chen, *Appl. Catal. B: Environ.,* 2022, **306**, 121065.

S10 R. T. Guo, Z. X. Bi, Z. D. Lin, X. Hu, J. Wang, X. Chen and W. G. Pan, *J. Colloid Interf. Sci.,* 2022, **627**, 343-354.

S11 L. L. Huang, S. P. Mo, X. Zhao, J. J. Zhou, X.B. Zhou, Y. N. Zhang, M. M. Fu,

Y. M. Fan, Q. L. Xie, D. Q. Ye, Y. F. Chen, *Chem. Eng. J.,* 2023, **474**, 145740.

S12 S. H. Guo, R. T.Guo, Z. R. Zhang, L. Q. Yu, J. S. Yan, H. Liu, W. G. Pan, X. J. Liu, *Sep. Purif. Technol.,* 2025, **354**, 129449.